Laser beam to the moon through the atmosphere

PHY204 - Project P05b

Aayam Basnet[a], Shreeya Upadhyay[b], Tamar Tsikarishvili[c], and Manon Pawlowski[d]

Abstract. In this project, we studied and modeled low-intensity laser propagation through the Earth's atmosphere. Employing a diverse set of simulation techniques, we analyzed the beam's propagation through different atmospheric conditions, ultimately projecting it towards the lunar surface.

Contents

1 Introduction

The subject of this report is the simulation of laser beam propagation to the Moon, with a particular focus on the atmospheric effects that influences this process. This project aims to understand how Earth's atmosphere impacts the transmission of a laser beam over such a vast distance, addressing key questions about the distortion and attenuation effects induced by atmospheric turbulence and diffraction. These

[a] aayam.basnet@polytechnique.edu
[b] shreeya.upadhyay@polytechnique.edu
[c] tamar.tsikarishvili@polytechnique.edu
[d] manon.pawlowski@polytechnique.edu

questions are particularly interesting as they can relate to both theoretical and practical aspects of space communication and optics-based lunar exploration.

In this project, we have developed different simulation methods that take into account several concepts from classical electrodynamics and optics such as the propagation of electromagnetic waves, the interaction of light with matter, and the principles of diffraction and refraction. In particular, since we are primarily dealing with optical lasers, there is a focus on phase of the wave, and how it changes on interaction with the atmosphere.

More specifically, we use Maxwell's laws to generate a wave equation, which we then constrain with the paraxial approximation, as demonstrated in subsection 2.1 to get the following equation:

$$2ik\frac{\partial E}{\partial z} = \nabla_T^2 E + k^2(n^2 - 1)E \tag{1}$$

Here E represents the complex wave, z is the propagation axis, ∇_T^2 is the transverse Laplacian, k is the angular wavenumber, and n is the index of refraction.

This equation is quite similar to the diffusion equation or the heat equation, and we solved it numerically using the algorithms that are used heavily for solving these equations: the spectral method[4] (described in subsection 3.1) and the Crank-Nicolson method[14] (described in subsection 3.4).

We relied heavily on the ideas presented in references [5] and [2] for general propagation to the moon, and more specifically, on references [5] and [10] for incorporating atmospheric effects. We developed simulations of gaussian lasers of various wavelengths and widths over various atmospheric conditions. Generally, we find that there is nothing stopping the light of a laser from reaching the Moon, although for most lasers, the light which would reach the Moon would be very low in intensity and highly spread out. However, the presence of atmospheric turbulence imparts seemingly random noise into the signal yielding noisy waves that reach the moon. Furthermore, the presence of clouds[17] and other solids in path of propagation causes scattering, reflection or absorption of the laser, completely preventing the propagation.

Since our propagation equation does not deal with high intensity lasers ($> 10^{10}$ Wm^{-2}), the question about the shape and behaviour of a high intensity laser through the atmosphere and towards the moon still remains. Furthermore, the value that describes the amount of atmospheric turbulence has a lot of variance depending on the time, season, temperature, and other factors that we have not considered. Further investigation is required for a more accurate model.

2 Theory

2.1 Paraxial Approximation of Propagation

The paraxial approximation (Equation 1) assumes that the beam's direction of propagation (say along the z-axis) is much more significant than the transverse directions (x and y directions). This approximation simplifies the analysis of the beam's behavior. This results in a simpler wave equation that is well-suited for long-distance propagation of light beams, and most specifically, has Gaussian solutions which approximates laser beams well.

In this derivation, z is taken to be the propagation axis, and $T = (x, y)$ is the transverse plane.
Starting with the scalar wave equation:

$$\frac{1}{c^2(x,y,z)}\frac{\partial^2 u}{\partial t^2} - \Delta u = 0 \tag{2}$$

Where u denotes the field of the wave we are considering. Taking its Fourier transform in time we get the Helmholtz equation.

$$\Delta\hat{u} + k^2 n^2(x,y,z)\hat{u} = 0 \tag{3}$$

with,

$$\hat{u}(x,y,z,\omega) = \int dt e^{-i\omega t} u(t,x,y,z)$$

Where $k = \omega/c_0$ is the angular wavenumber, c_0 is the reference speed: the speed of light, $c(x, y, z)$ is the propagation speed, and $n(x, y, z) = c_0/c(x, y, z)$ is the index of refraction. We consider the beam to be in the narrow regime i.e. we consider the propagation of the beam to be in only one direction throughout. Thus, in the narrow beam regime we can apply the paraxial approximation. We write the solution of the Helmholtz equation in the form:

$$\hat{u}(x, y, z, k) = e^{-ikz}\,\mathrm{E}(x, y, z, k) \tag{4}$$

Here, E is the envelope of the propagating field. The use of this solution in Equation 3 leads to:

$$-2ik\frac{\partial \mathrm{E}}{\partial z} + \frac{\partial^2 \mathrm{E}}{\partial z^2} + \Delta_T \mathrm{E} + k^2(n^2 - 1)\mathrm{E} = 0.$$

Assuming that the function E is slowly varying in z so that:

$$k\left|\frac{\partial \mathrm{E}}{\partial z}\right| \gg \left|\frac{\partial^2 \mathrm{E}}{\partial z^2}\right|$$

We thereby obtain a parabolic equation for the envelope:

$$2ik\frac{\partial \mathrm{E}}{\partial z} = \Delta_T \mathrm{E} + k^2(n^2 - 1)\mathrm{E} \tag{5}$$

An important thing to note is that in Equation 4, we could have instead taken e^{ikz} instead of e^{-ikz}, depending on the propagation direction. This will lead to a difference in the sign of the coefficient of the $\frac{\partial E}{\partial z}$ term. However, this does not affect the solution that we receive since we shall only be taking the real part of the solution or the intensity, this sign change, that affects the imaginary part of the solution will not impact our results.

We provide a more detailed overview of the proof for paraxial approximation, accounting for the scalar approximation and polarization in Appendix B

2.2 Gaussian optics

This section heavily references [12] in its theory and derivations. Light beams where the electric field profile in a plane perpendicular to the beam axis can be described with a Gaussian function, possibly with an added parabolic phase profile, are called Gaussian beams. We consider these beams to be the fundamental mode or the transverse Gaussian mode TE_{00}, which implies that they diverge less and can be focused better than other beams.

The Gaussian function is infinite in extent, however this is not true in reality as perfect Gaussian beams do not exist in nature. Still, the Gaussian beam is a useful model for the beam in cases where the lenses or mirrors in the beam are significantly larger than the spot size $w(z)$ of the beam. Here $w(z)$ represents the beam radius at the point z from the origin.

Gaussian beams are usually considered in situations where the beam divergence is relatively small, so that the so-called paraxial approximation Equation 1 can be applied (here beam divergence or the beam divergence angle of a laser beam is a measure for how fast the beam expands far from the beam waist in the far field. It is important to note that the beam divergence is not a local property of a beam, i.e. for a certain position along its path, but a property of the beam as a whole.). Thus, owing to subsection 2.1, this approximation allows the omission of the term with the second-order derivative in the propagation equation, so that a first-order differential equation results.
Within the paraxial approximation, a Gaussian beam propagating in free space (or in a homogeneous medium) remains Gaussian, except that of course its parameters evolve. For a monochromatic beam of wavelength λ propagating in the direction $+z$, the electric field given by the solution of the propagation equation is:

$$E(r, z) = E_0\frac{w(z)}{w_0}\exp\left(\frac{-r^2}{w^2(z)} + i\frac{kr^2}{2R(z)} - i\zeta(z)\right) \tag{6}$$

here $|E_0|$ is the peak amplitude, w_0 is the beam waist radius, and $w(z)$ is the beam radius at distance z from the focus (point where beam radius is w_0 and minimal).

Due to diffraction, the beam radius changes with the propagation direction. The beam radius is defined as:

$$w(z) = w_0\sqrt{1 + \frac{z^2}{z_R^2}} \tag{7}$$

Here the z_R is the Rayleigh length which is defined as $z_R = \frac{\pi w_0^2}{\lambda}$. The position $z = 0$ in the equation above corresponds to the beam waist or the focus where the beam radius is at its minimum, and the phase profile is flat.

The radius of curvature R(z) of the wavefronts evolves according to the equation:

$$R(z) = z + \frac{z_R^2}{z} \tag{8}$$

At the beam waist where $z = 0$ the radius of curvature $R(z)$ is infinite, meaning the wavefronts are planar. As the beam propagates away from the waist, the wavefronts become increasingly curved. For $z \gg z_R$, the radius of curvature $R(z)$ approximates z, indicating that the wavefronts become nearly spherical. Moreover, a positive $R(z)$ means that the wavefronts are convex, or bending away from the direction of propagation. This curvature of the wavefronts is a key feature of Gaussian beams, influencing how the beam focuses and diverges as it travels through space.
The transverse profile of the optical intensity of the beam with an optical power P can be described with a Gaussian function.

$$I(r, z) = \frac{2P}{\pi w^2(z)} \exp\left(\frac{-2r^2}{w^2(z)}\right) \tag{9}$$

Here the beam radius $w(z)$ is the distance from the beam axis where the intensity drops to $1/e^2$ of the maximum value. This characteristic makes $w(z)$ a crucial parameter for describing the beam's spatial extent and its divergence properties. Additionally, the full width at half maximum (FWHM) of the intensity profile, which is the width at which the intensity drops to half of its peak value, is approximately 1.18 times the beam radius $w(z)$. This relationship provides a useful measure for comparing the spread of the beam's intensity with other beam profiles.

2.3 Atmospheric Effects

The atmosphere is most famously modeled with a quadratic form of the index of refraction depending on the height. The US standard atmosphere (1962) models this behaviour by the following formula[8]:

$$n(z) = 1 + A + Bz + Cz^2 \tag{10}$$

Where z denotes the vertical height in km, and the constants A, B and C have the following values:

$$\begin{aligned} A &= 0.000321 \\ B &= -0.00003670 \\ C &= 0.000001350. \end{aligned}$$

However, this model assumes there are no transverse changes in the the index of refraction, which is not true for the real atmosphere. Turbulence effects caused by the interaction between hot and cold air, jet streams, and other structures like mountains create minute changes in the transverse index of refraction. Hence, we will have to consider $n(x, y, z)$ instead of merely $n(z)$ for a more accurate model of propagation.

2.3.1 Modeling turbulence in the atmosphere using phase screens

The phase-screen method is a technique for modelling the transmission of waves in some media. The model can be considered as a series of thin lenses or diffraction "screens" that are orthogonal to the principle direction of propagation. A monochromatic wavefront travelling through a homogeneous medium interacts with a lens-like screen, that modifies the phase and amplitude of the wavefield. Part of the incident wavefield emerges from the screen as a more complicated field and travels forward through the subsequent homogeneous region with some subsequent screen. Part of the incident wavefield is reflected

back towards the source where it can also undergo interactions or be observed at some previous screen.

This method is useful for constructing a mathematical model because knowing the field values over any screen in the model is sufficient to determine the field values over any subsequent screen. This is due to the one-directional wave assumption and the use of a complex representation for the field. The field observed on a single screen can be decomposed into its different spatial frequencies using a Fourier transform. Such a decomposition is equivalent to decomposing the monochromatic field into components traveling at different angles to the screen. Predicting the field on a subsequent observation screen involves phase-shifting each angular component by the appropriate amount to correspond to the distance that a ray at its particular angle must travel to reach the next screen. In particular, this method applied to our model only changes the phase of the wave and leaves the amplitude unchanged. More about phase screens can be found in this reference[18].

For modeling turbulence, we assume uniformly spaced phase screens at every z_n over the propagation axis and denote $\Delta z = z_{n+1} - z_n$. In each phase screen, we then use the relation between the power spectral density due to turbulence (ϕ_θ), and the refractive index spectrum (ϕ_n)[10]:

$$\phi_\theta(\kappa) = 2\pi k^2 \Delta z \phi_n(\kappa) \tag{11}$$

Here, $\kappa = (k_x, k_y)$, the transverse axes in Fourier space.
The quantity ϕ_n can be approximated by a variety of different models: pure power law, inner scale cutoff, outer scale cutoff, etc. For our model, we used the outer scale cutoff model due to the distances we are working on. This model is of the von Karman type[16]:

$$\phi_n(\kappa) = K(\alpha) C_n^2 (\kappa^2 + 1/L_0^2)^{-\frac{\alpha}{2}-1}$$

Where L_0 denotes the parameter representing the outer scale. This is a difficult parameter to estimate, and there are conflicting reports[7]. C_n^2 is a parameter that gives information about the amount of turbulence in the atmosphere. It is highly dependent upon the time, temperature, weather, location, season, and a myriad of other factors. There are different estimations in these references[13][1][6]. We used different values to demonstrate the effect in the wave in variety of conditions. In general, $C_n^2 \sim 10^{-15}$ corresponds to the normal breezy weather over the first kilometer of altitude. This value decreases as the altitude increases, and we have taken estimations regarding the same in our simulations. More shall be discussed in the section 4. $K(\alpha)$ is the standard Kolmogorov spectrum for $\alpha = 5/3$, so that $K(5/3) = 0.033$[10].

3 Simulation method

3.1 Spectral Method:

Rewriting the propagation equation 1, for $n = 1$, so that $k^2(n^2 - 1)\mathrm{E} = 0$:

$$\frac{\partial^2 \mathrm{E}}{\partial x^2} + \frac{\partial^2 \mathrm{E}}{\partial y^2} - 2ik\frac{\partial \mathrm{E}}{\partial z} = 0 \tag{12}$$

We introduce the Fourier transform of E:

$$\hat{\mathrm{E}}(k_x, k_y, z) = \int_{-\infty}^{\infty}\int_{-\infty}^{\infty} \mathrm{E}(x, y, z)\exp(-i(k_x x + k_y y))\mathrm{dxdy} \tag{13}$$

Applying this transformation in Equation 12, we get:

$$2ik\frac{\partial \hat{\mathrm{E}}}{\partial z} = -(k_x^2 + k_y^2)\hat{\mathrm{E}} \tag{14}$$

This is a simple differential equation, that can be solved by the separation of variables to obtain:

$$\hat{\mathrm{E}}(k_x, k_y, z) = \hat{\mathrm{E}}(k_x, k_y, 0)\exp\left(-\frac{k_x^2 + k_y^2}{2ik}z\right) \tag{15}$$

Then, we apply an inverse Fourier transform which allows us to find the solution:

$$\mathrm{E}(x, y, z) = \frac{1}{2\pi}\int_{-\infty}^{\infty}\int_{-\infty}^{\infty} \hat{\mathrm{E}}(k_x, k_y, z)\exp(i(k_x x + k_y y))\mathrm{dk}_x\mathrm{dk}_y \tag{16}$$

Algorithm:
We discretize space into a two dimensional grid. The extent of this grid shall be our boundary condition. For each grid, we have assigned a certain value corresponding to the average of the electric field over the space of the grid. Let us denote any random gridpoint as U. To get $E(x, y, z)$ from $E(x, y, z = 0)$, therefore, we have to get $U(x, y, z)$ from $U(x, y, z = 0)$ for each U. We used the following algorithm for the same:

1. Initialize the initial condition ($E(x, y, z = 0)$) in a grid that has been defined within the boundary conditions. Below, we list the steps for every gridpoint represented by U.
2. Calculate $\hat{U}(k_x, k_y, 0)$ by doing a discrete fourier transform (FFT2: `numpy.fft.fft2`) to $U(x, y, 0)$
3. Use the Equation 15 to have:

$$\hat{U}(k_x, k_y, z) = \hat{U}(k_x, k_y, 0) \exp\left(-\frac{k_x^2 + k_y^2}{2ik} z\right)$$

   Here, k_x and k_y are the points in the transverse spectral grid calculated using $2\pi\times$`numpy.fft.fftfreq`. The 2π factor comes since we are using angular wavenumbers.
4. Calculate $U(x, y, z)$ by doing an inverse discrete fourier transform (IFFT2: `numpy.fft.ifft2`) to $\hat{U}(k_x, k_y, z)$

Usually, to have more stability in the scheme, we perform step 2 in small steps Δz over the propagation distance.

3.2 Split step method

The previous section dealt with situations where $n = 1$. However, if this is not the case, we will need to use the split step method to solve the propagation equation. As mentioned above, for this method, we will perform the algorithm in small steps, so that if $\mathrm{E}_n(x, y)$ is the solution at $z = z_n$, then $\mathrm{E}_{n+1}(x, y)$ is the solution at $z_{n+1} = z_n + \Delta z$[5]:

$$\mathrm{E}_{n+1} = \exp\left[-\frac{i}{2k}\left(\Delta z \nabla_T^2 + k^2 \int_{z_n}^{z_{n+1}} (n^2 - 1) dz\right)\right] \mathrm{E}_n \tag{17}$$

For small Δz, $(n^2 - 1) \approx$ constant. Therefore the integral in the exponential can be written as the following:

$$k^2 \int_{z_n}^{z_{n+1}} (n^2 - 1) dz \approx k^2 (n^2 - 1) \int_{z_n}^{z_{n+1}} dz = k^2 (n^2 - 1) \Delta z \tag{18}$$

Thus, we get:

$$\mathrm{E}_{n+1} = \exp\left(-\frac{i}{2k} \Delta z \nabla_T^2\right) \exp\left(-\frac{i}{2} k (n^2 - 1) \Delta z\right) \mathrm{E}_n \tag{19}$$

We already know what the value $\exp\left(-\frac{i}{2k} \Delta z \nabla_T^2\right) \mathrm{E}_n$ is from the spectral method described in the previous section. Let us denote this solution as $\tilde{\mathrm{E}}_{n+1}$, yielding:

$$\mathrm{E}_{n+1} = \tilde{\mathrm{E}}_{n+1} \exp\left(-\frac{i}{2} k (n^2 - 1) \Delta z\right) \tag{20}$$

Note that this explanation is not the most rigorous. The proof of why this process works is much more involved and is well-explained in reference[5].

With this in mind, implementing this boils down discretizing the space as before. Let us denote the field at any random gridpoint at $z = z_n$ as U_n. Therefore, to get E_{n+1} from E_n, we have to get U_{n+1} from U_n for every gridpoint. The algorithm steps after the initialization of the grid and the initial condition are listed below:

1. Calculate $\hat{U}(k_x, k_y, z_n)$ by doing a discrete fourier transform (FFT2: `numpy.fft.fft2`) to $U(x, y, z_n)$
2. Use the Equation 15 to have:

$$\hat{U}(k_x, k_y, z_{n+1}) = \hat{U}(k_x, k_y, z_n) \exp\left(-\frac{k_x^2 + k_y^2}{2ik} \Delta z\right)$$

   Here, k_x and k_y are the points in the transverse spectral grid calculated using $2\pi\times$`numpy.fft.fftfreq`.

3. Calculate $\tilde{U}(x, y, z_{n+1})$ by doing an inverse discrete fourier transform (IFFT2: `numpy.fft.ifft2`) to $\hat{U}(k_x, k_y, z_{n+1})$
4. Mutiply the obtained $\tilde{U}(x, y, z_{n+1})$ by $\exp\left(-\frac{i}{2}k(n^2-1)\Delta z\right)$ to obtain $U(x, y, z_{n+1})$

3.3 Phase Screen Method:

The concept of phase screen has been explained in subsubsection 2.3.1. The basic reason why this works is also very similar to the split step method. However, instead of making the approximation in Equation 18, we have the integral approximated by $\phi_\theta(\kappa)$ mentioned in Equation 11 acting over a larger Δz. However, this quantity is in the Fourier space and does not encapsulate the randomness of the turbulence of the atmosphere. It only gives information about the average phase change that will be imparted to the wave. Specifics about how to work with this quantity is in the following subsection.

3.3.1 Utilization of Phase Screens

We recall Equation 11

$$\phi_\theta(\kappa) = 2\pi k^2 \Delta z \phi_n(\kappa)$$

In order to randomize our function we generate random a 2D array of complex numbers $(A_{jn} + iB_{jn})$, with the size of the array corresponding to the gridpoints of the spectral method. Here, A_{jn} and B_{jn} are independent randomly generated integers following a normal distribution with mean 0 and variance 1. Accurately modeling the chaotic nature of turbulence is not currently possible. So, we shall use these pseudorandom numbers to obtain a model of the effect.

These numbers are then multiplied to $\Delta_k^{-1}\sqrt{\Phi_\theta(j\Delta_k, n\Delta_k)}$, where $\Delta_k = 2\pi/N\Delta$ where Δ represents $dx = dy$, the transverse grid length and N represents the number of gridpoints.

Defining P_0 as $P_0 = (A_{jn} + iB_{jn})\Delta_k^{-1}\sqrt{\phi_\theta(j\Delta_k, n\Delta_k)}$, we calculate P as the following:

$$P = \frac{2\pi}{dxdy}\texttt{ifft2}(P_0) \tag{21}$$

Since P is a complex number, we write $P_{real} = Re(P)$ and $P_{imag} = Im(P)$. P_{real} and P_{imag} represent the phase that should be added to the wave at two different phase screens.

For instance, we can have:

$$\begin{aligned} U(x, y, z_n) &= \tilde{U}(x, y, z_n)\exp(iP_{real}) \\ U(x, y, z_{n+1}) &= \tilde{U}(x, y, z_{n+1})\exp(iP_{imag}) \end{aligned} \tag{22}$$

Here, the symbols represent the same thing they did in the previous section, with the algorithm till step 3 the same as that of phase screens. One thing to note is that phase screens are placed with higher distances between them. There may be a number of steps within two phase screens to propagate the wave without the effect of atmosphere at all. Each phase screen is supposed to add the effect of the entire atmosphere between two phase screens at once. For our implementation, we have used phase screens every 20 m, and have only used P_{real} every time, discarding P_{imag}. Figure 1 shows us the the parameter P_{real} for an arbitrary phase screen for $C_n^2 = 10^{-14}$ m$^{-2/3}$.

3.3.2 Normalization of units and Parseval's Equality

While going through the process described above, we only go through `ifft2`, and do not use `fft2`. This means that we will need to pay attention to the standard scaling, and the continuous to discrete approximation. This process is called normalizing.

As shown in the above subsection we have defined $P = \frac{2\pi}{dxdy}\texttt{ifft2}(P_0)$. We actually obtained the coefficient using relation between the theoretical continuous Fourier transforms, and the computational discrete one.

For a function $f(\mathbf{r})$ and its Fourier transform $\hat{F}(\kappa)$, its inverse Fourier transform is:

$$f(\mathbf{r}) = \frac{1}{2\pi}\int_{-\infty}^{\infty}\int_{-\infty}^{\infty}\hat{F}(\kappa)e^{i\kappa\cdot\mathbf{r}}dk_x dk_y \tag{23}$$

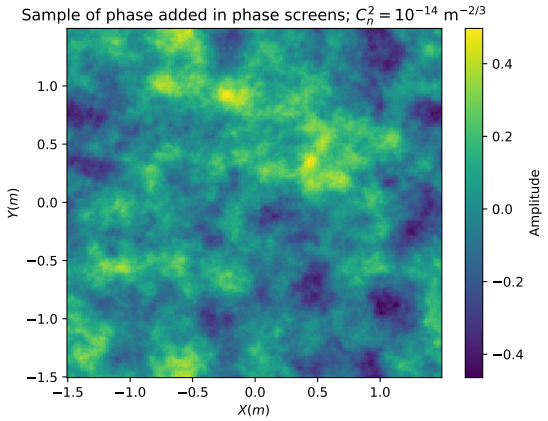

Fig. 1. The profile of parameter P at an arbitrary phase screen for $C_n^2 = 10^{-14} m^{-2/3}$

This equation can be approximated to its discrete counterpart:

$$f(\mathbf{r}) \approx \frac{1}{2\pi} \Delta k_x \Delta k_y \sum\sum \hat{F}(\kappa) e^{i\kappa\cdot\mathbf{r}} \tag{24}$$

Since by construction, $\Delta k_x = \frac{2\pi}{N_x dx}$ and $\Delta k_y = \frac{2\pi}{N_y dy}$, we get:

$$f(\mathbf{r}) \approx \frac{1}{2\pi} \frac{2\pi}{N_x dx} \frac{2\pi}{N_y dy} \sum\sum \hat{F}(\kappa) e^{i\kappa\cdot\mathbf{r}} \tag{25}$$

which gives us

$$f(\mathbf{r}) \approx \frac{2\pi}{dxdy} \left(\frac{1}{N_x N_y} \sum\sum \hat{F}(\kappa) e^{i\kappa\cdot\mathbf{r}} \right) \tag{26}$$

The expression inside the bracket, according to documentation is the inverse Fourier transform in `numpy`:

$$f(\mathbf{r}) \approx \frac{2\pi}{dxdy} \texttt{ifft2}(\hat{F}(\kappa)) \tag{27}$$

In our model, since $dx = dy$, we therefore obtain the coefficient in Equation 21.

To check if our calculations are correct, we checked that the Parseval-Plancherel theorem between P and P_0 was satisfied:

$$\int P_0 dk_x dk_y = \int P dx dy \sim \sum (P_0 \Delta k_x \Delta k_y) = \sum (P dx dy) \tag{28}$$

3.4 The Crank-Nicolson Method

The Crank-Nicolson method is a finite difference method for solving a differential equation. It works by approximating the derivatives with finite differences. The space is discretized and the values of the solution at the end points of the intervals are approximated by solving algebraic equations containing finite differences and values from nearby points.

This amounts to solving a system of linear equations to obtain the solution at every step of the propagation, making this scheme highly time and computation intensive. However, since this is an implicit scheme (finding a solution by solving an equation involving both the current state of the system and the later one), the error is bounded, and therefore is numerically stable for longer distances. However, having a two dimensional wave without rotational symmetry is more complicated to implement with this scheme. For a 2D noisy gaussian, the basic and naive implementation is only able to propagate a 1D slice.

This method has been well explained by team 3 (group-5A) in their report and presentation and in the reference[17].

3.5 Change of Coordinates

Simulating the entire distance to the moon without any consideration results in a high error in the final result due to the limited range considered for the transverse axis. This limited range acts like a wave guide, limiting the transverse extent of the wave resulting in a wave like the one in Figure 3. However, such limitations do not exist in reality. Therefore, to remedy this, we implement a change of coordinates that scales with the width of a standard gaussian propagation in the transverse direction. The change of coordinates are given below:

$$\begin{aligned} \zeta &= \tan^{-1}(\tilde{z}) \\ \xi &= \frac{\tilde{r}}{\tilde{w}(\tilde{z})} \end{aligned} \tag{29}$$

Where, the tilde are due to normalizing the parameters as

$$\tilde{z} = (z/z_R),$$

$$\tilde{r} = r/w_0 = \sqrt{x^2 + y^2}/w_0,$$

$$\tilde{w}(\tilde{z}) = \sqrt{1 + \tilde{z}^2}.$$

On top of this change, we will need to change the normalized electric field to computational space as well. This is done by removing the standard phase and multiplying by the normalized radius:

$$C = E(\tilde{r}, \tilde{z})\tilde{w}(\tilde{z}) \exp\Big(-i\tilde{r}^2/\tilde{R}(\tilde{z}) + i\zeta(\tilde{z})\Big) \tag{30}$$

Here the normalized radius of convergence is $\tilde{R}(\tilde{z}) = \tilde{z} + 1/\tilde{z}$.
With these changes, the propagation equation turns into the following:

$$\frac{\partial C}{\partial \zeta} = \frac{i}{4}\nabla_\xi^2 C + i[1 - \xi^2]C \tag{31}$$

A more through look into why and how this works is well explained by team 3.
An algorithm to use this process with the spectral is given below:

1. Transform the initial wave into computational space: $E(z, r)$ to $C(\zeta, \xi)$. We need to ensure the scaling of the axes that the wave should be $\sim C \exp\big(-\xi^2\big)$
2. Advance C up to a propagation distance ζ using the spectral method, and having the $i[1 - \xi^2]C$ term implemented using the split step method described in subsection 3.2.
3. Transform C back into physical space using the scaling provided in Equation 29 and Equation 30.

The $i[1 - \xi^2]C$ term here acts as a refractive index profile that will guide the beam within the computational box. For a perfect gaussian, its shape should remain constant throughout its propagation in the computational space.

However, the addition of noise through atmospheric turbulence will introduce additional complexities. Since the method only prevents the perfect gaussian from expanding, the noise will still expand outwards. Since we have initially defined a finite boundary condition, the edges of this boundary act as a wave guide, reflecting back the noise to the wave. Since the noise is random, they will randomly interact with each other, giving a result that is false for our experiment. Therefore, we implement a filtering algorithm that shall be explained in the following subsection.

3.6 Boundary noise filtering

As mentioned in the previous section, the boundary conditions acting as a wave guide messes up with our signal. To prevent this, we create a border near the boundary that absorbs any wave that comes near it.

One should notice that such a measure is not possible if the wave is not in the computational space. In real space, since the width of the gaussian wave itself increases, we will be filtering out our signal if we were to implement this. However, implementing such an absorption in the computational space would only affect the noise since the actual Gaussian should remain unchanged throughout propagation in this space due to the $i[1 - \xi^2]C$ term. We could keep increasing the boundary conditions to account for the

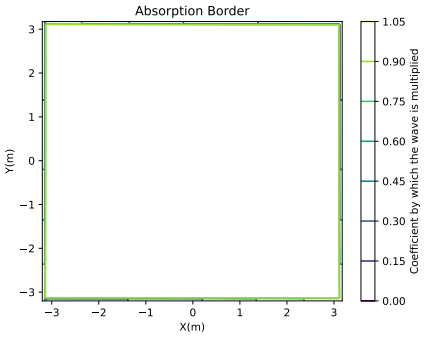

Fig. 2. Border created by the absorption coefficient

noise, but it will get very computationally expensive, and the actual beam will comparatively be narrower in that scale.

Therefore, we have implemented an absorption coefficient within three gridlines closest to the edge of the grid in computational space. An image representing this absorption is shown in Figure 2.

The algorithm to achieve this, and propagate the wave in computational space using this technique is listed below.

1. The first step remains the same as subsection 3.5
2. For each step in the propagation of C as defined in step two of subsection 3.5, we will add an additional term. After multiplying by the refraction term as a phase, we multiply C again by a mask represented by Figure 2.
3. Step 3 also remains the same as before

The creation of this mask Figure 2 involves creating an grid of ones, and having exponentially decaying functions in the borders. An implementation is shown in the github referenced in the appendix.

4 Results and Discussion

4.1 Preliminaries

Our results show that the laser beam will propagate to moon in the absence of obstruction although the laser intensity may be diminished and the beam reaching the moon might be highly distorted.

Throughout our project we consider the initial amplitude of the beam to be equal to 1 NC^{-1}, thus, if our beam were to differ in amplitude from this value, we can simply multiply the resulting array with the required beam amplitude. In our simulations, we dynamically adjust the size of the simulation

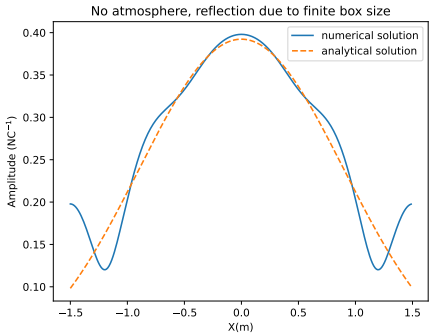

Fig. 3. Error in simulation due to limited grid extent

box to account for the increasing propagation distance of the beam. However, when this adjustment is neglected, it will lead to errors, as illustrated in Figure 3 which shows the amplitude of the laser beam at a significant distance from the origin without any changes in the box size. The edges of the grid

acting as a waveguide destroys the shape of the Gaussian, diverging it significantly from its analytical counterpart. This discrepancy underscores the critical importance of incorporating the evolving box size (subsection 3.5) into our simulations to ensure alignment with theoretical predictions.
We initially simulated the propagation of the beam to the moon without the presence of any atmospheric effect. We can observe in Figure 4 that the laser beam exactly matches with the analytical solution of the Gaussian.

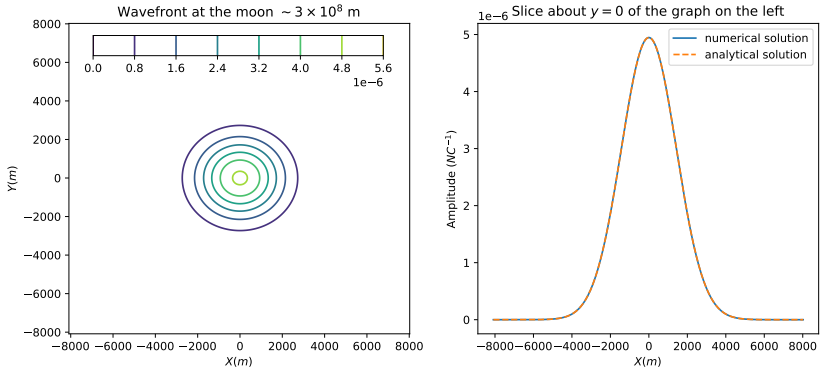

Fig. 4. The contour plot as well the the amplitude profile for a laser beam of initial radius 0.01 m in absence of any atmospheric effect when it reaches the moon

The next step consisted of modeling the atmospheric effects through change of refractive index in the propagation axis (Equation 10) through the use of the split step method. However, we observed that the effects caused by this model is negligible over the distance of the atmosphere. Therefore, we focus only on the turbulence effects for the rest of this section.

4.2 Turbulence

It is important to note here that we have considered our laser to have a $50cm$ radius for the rest of our simulations. Our motivation for choosing this value is to have a stable beam radius for the entirety of the atmosphere. Choosing a larger radius allows the beam divergence to be smaller which helps us to simulate the beam for very large distances using the same grid, and therefore reducing computational intensity and time. We are allowed to use such a beam since the paraxial approximation still holds well for these sizes.

However, this is not very practical size as increasing the laser diameter makes it more difficult to maintain the coherence of the beam. Moreover, it is also difficult to construct or maintain such a laser. Although the world's largest laser has a diameter of $10m$ but it is not a commercially available laser.[9]

As defined in subsubsection 2.3.1, C_n^2 is a parameter that gives information about the amount of turbulence in the atmosphere. We observe after the implementation of the phase screen method, varying the values of C_n^2 for $C_n^2 \leq 10^{-13}\, m^{-2/3}$ the beam is significantly distorted due to noise. This however does make sense as the turbulence effects are stronger for $C_n^2 \leq 10^{-13}\, m^{-2/3}$ which might explain this influence on the beam

In comparison to Figure 4 we see in Figure 6that for only $25km$ distance from the origin, our beam deviates significantly from the analytical solution. Although the average beam still remains a Gaussian, in accordance with our expectation, the atmospheric effects indeed influence our beam propagation.
After we propagate our beam to the moon we come across the problems as mentioned in 3.6. Accordingly, we implement the filtering method by absorption of noise in the computational space. We can see in Figure 7 that our numerical solution has noise due to turbulence effects. After implementing the absorption of noise, we see in Figure 8 that the noise from our numerical solution indeed gets filtered. The solution however, is not exactly equal to the analytical solution, but we expect this to be the effect of the atmospheric turbulence.

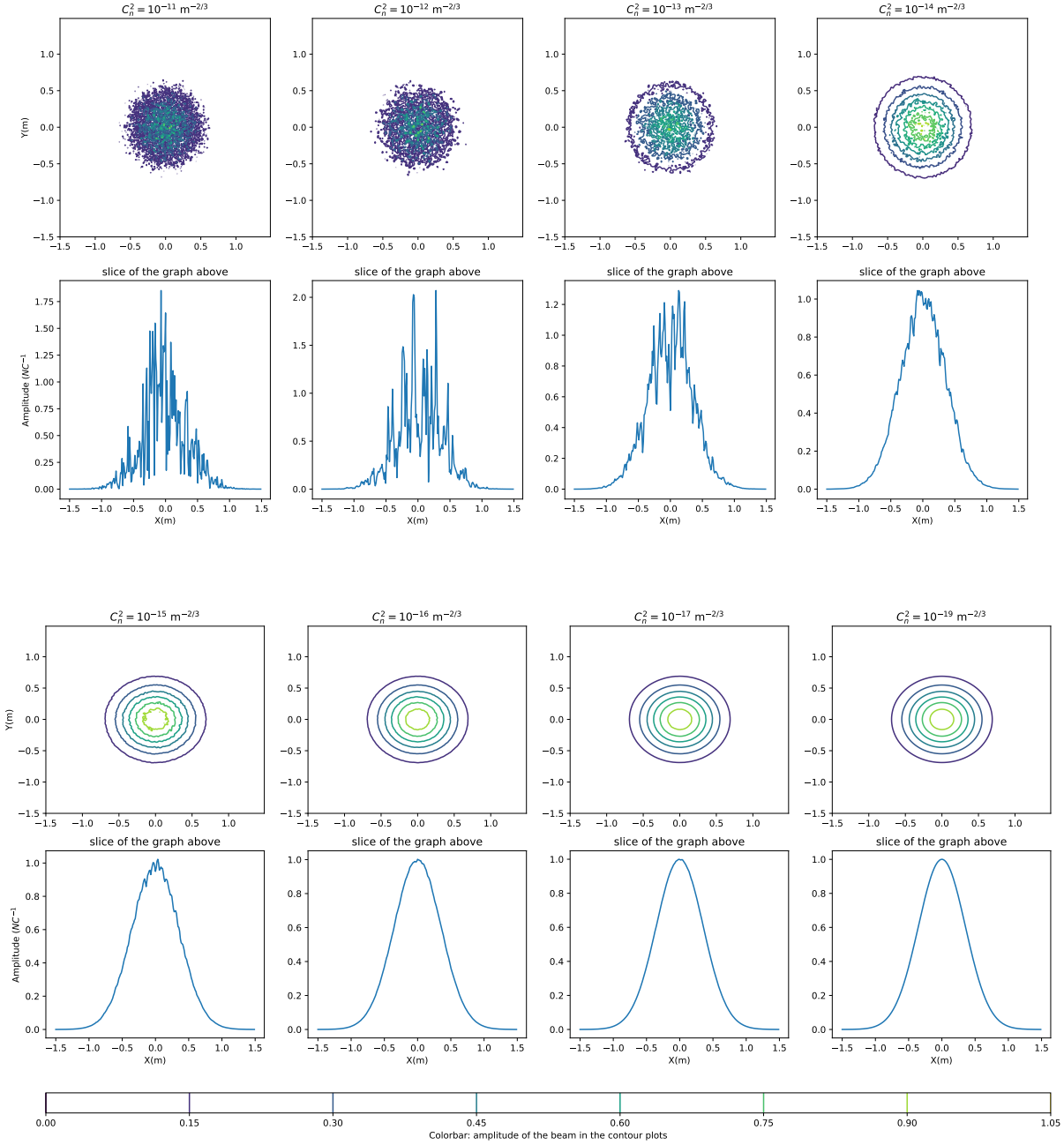

Fig. 5. Plot showing the beam amplitude profile with a phase screen every 20m and at 2.8km from the origin as a contour plot(above) with respect to the x-direction(below) for values of C_n^2 as indicated in the individual graphs

4.3 A discussion about detection

We would like to mention that as we are dealing with low intensity waves ($1.27\,Wm^{-2}$), the beam on reaching the moon might be highly diminished and distorted due to the noise added due to the presence of external sources. In case a detector is placed on moon to measure the incoming signal, it would be essential that the average signal over a significant amount of time has a well defined phase. Although the analytical solution gives a constant phase for the propagating beam at a given distance from the focus, due to the addition of noise by atmospheric turbulence, we see that a random phase is also added to the propagating beam. However, this random phase will not play a significant role in the signal detection if the detection is done for a sufficiently large time frame, it will not contribute to the average signal. Similarly, the external noise will average out if the average signal has a well defined phase over a significant time frame.

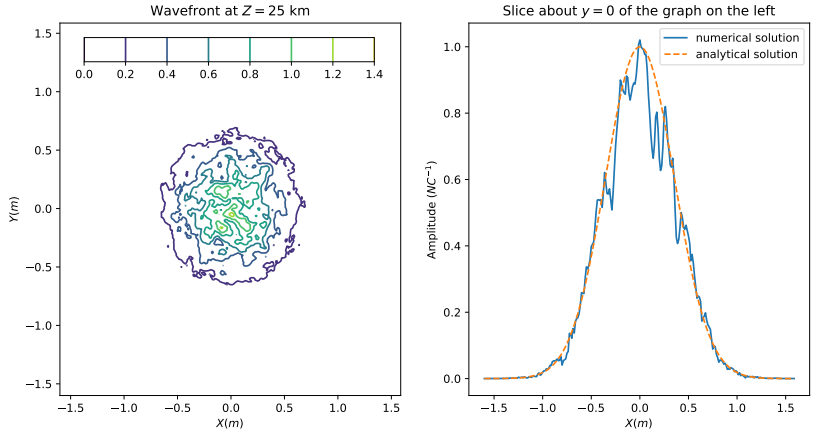

Fig. 6. The contour plot as well the the amplitude profile for a laser beam at $z = 25km$; with $C_n^2 = 10^{-15}$ for the first $1km$, 10^{-17} for the $8km$ after, and 10^{-18} for the last $16km$

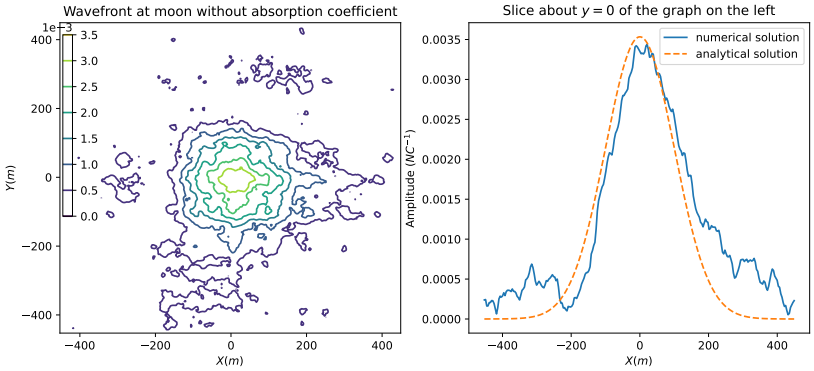

Fig. 7. The contour plot and beam profile for the beam amplitude for the beam at moon without implementing filtering the noise by absorption for the beam in Figure 6. Notice that the noise profile in the tail ends are similar to each other, which is likely due to the noise reflecting off the edge of the grid

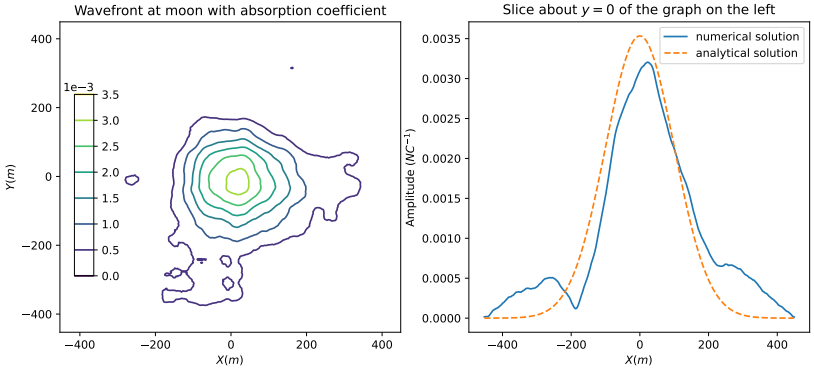

Fig. 8. The contour plot and beam profile for the beam amplitude for the beam at moon after implementing filtering the noise by absorption for the beam in Figure 6.

4.4 Application

Laser beam propagation has multiple applications in real life. It is the central point of Lunar Laser Ranging (LLR) experiments, a practice in lunar astronomics. Moreover, the distance between the moon and the Earth has been measured by laser ranging since 1962. The method has then been improved thanks to *Apollo 11, 14, 15* and *Lunokhod 1, 2* missions, which set reflectors on the surface of the moon

More than measuring the Earth-Moon distance, LLR measurements allowed scientists to make new discoveries about our satellite. Indeed, they discovered that it is slightly drifting away from the Earth, *i.e.* its orbit is getting larger every year.

5 Conclusions

In this project we studied the propagation of a laser beam through the atmosphere and the effects of the atmospheric conditions on the process. Our results show that without any obstruction in the path of the beams (clouds, satellites, dust particles, other scattering agents), the beam will reach the moon. However it will be highly diminished and distorted due to atmospheric turbulence.

We were able to learn about the different simulation methods such as split screen method, phase screen method, Crank-Nicolson method and implement them to simulate the propagation of the beam though the atmosphere and beyond. We were able to apply our theoretical knowledge regarding lasers, wave propagation as well as atmospheric effects and generate results which are in accordance with our expectation. However we can improve our implementation methods by trying to decrease the complexity and the runtime of our simulations.

A realistic extension could occur by introducing high intensity beams ($> 10^{15}$ Wm^{-2}). The utilization of high intensity lasers would cause the characteristic of the medium to change with respect to the beam propagation due to which the linearity of the polarization $\hat{P}$ doesn't hold (This assumption is explained in the appendix). This however is more realistic as the detection of low intensity beams is very difficult due to ambient noise, atmosphere, and the inherent lack of intensity. Another task would be to focus on the effects due to ions in the ionosphere, where the charged particles may interact with and influence beam propagation. One could also simulate the effect of other atmospheric effects as well. Extension of this project into non-optical wavelengths would also be an interesting undertaking.

Appendix

A Code

All the relevant code used for this simulation has been compiled into a jupyter notebook that is available in the following link:

`https://github.com/aayam2/PHY204-Laser_to_the_moon`

B Complete derivation of the paraxial approximation:

In the following, we shall derive the paraxial approximation for wave propagation (Equation 1) from the Maxwell-Faraday and Maxwell-Ampere laws in non-magnetic medium:

$$\boldsymbol{\nabla} \times \mathbf{E} = -\frac{\partial \mathbf{B}}{\partial t} \tag{32}$$

$$\boldsymbol{\nabla} \times \mathbf{B} = \mu_0(\mathbf{J} + \frac{\partial \mathbf{D}}{\partial t}) \tag{33}$$

Here, $\mathbf{E}$ and $\mathbf{B}$ denote the electric and magnetic fields respectively, $\mathbf{D}$ denotes the electric displacement field, $\mathbf{J}$ is the current density of free charges and μ_0 denotes the permeability of free space. All the terms depend on the space variables $\mathbf{r} = (x, y)$, the time taken t and the propagation variable z. In our case, we are assuming our beam to always be propagating along the z-direction.

We now define the polarization density: it is a vector field that describes how the bound charges in the medium responds to an applied electric field, as well as how the material changes the field. If we consider our medium: air, which usually does not have a permanent dipole, its polarization itself usually depends on the electric field of the wave.

We can decompose the polarization into a linear term $\mathbf{P}^{(1)}$ describing the response of the medium for weak electric fields and a non-linear term **P'** that is a nonlinear function of the electric field components and becomes relevant for stronger field.

In the range where most of the electrons in the medium are still bounded to the nucleus, we can take the approximate position that $\mathbf{P} \sim \mathbf{P}^{(1)}$. This approximation is valid for lasers of intensities up to $\sim 10^{15}$ Wcm^{-2}, below which ionization induced by the optical field leads to a plasma of smaller density than that of the neutral medium [2]. In our case, we consider air, which is an isotropic and homogeneous dielectric medium for which the component of the polarization field are linear component of the electric field. The polarization can then be written as:

$$\vec{\mathbf{P}}^{(1)}(\mathbf{r}, \omega, z) = \epsilon_0 \chi^{(1)}(\omega) \vec{\mathbf{E}}(\mathbf{r}, \omega, z) \tag{34}$$

where ϵ_0 denotes the permittivity of free space and $\chi^{(1)}(\omega)$ is the linear susceptibility, with a dependence on ω, which is the angular frequency.
We also have the expression for electric displacement:

$$\mathbf{D} = \epsilon_0 \epsilon(\omega) \mathbf{E} + \mathbf{P} \tag{35}$$

where $\epsilon(\omega) = 1 + \chi^{(1)}(\omega)$ which denotes the relative permittivity of the medium. Now by inserting Equation 35 in Equation 33, we get:

$$\boldsymbol{\nabla} \times \mathbf{B} = \mu_0 \left(\mathbf{J} + \frac{\partial(\epsilon_0 \epsilon(\omega) \mathbf{E} + \mathbf{P})}{\partial t} \right) \tag{36}$$

Then we apply the time derivative on both sides of Equation 36 to arrive to the following:

$$\boldsymbol{\nabla} \times \frac{\partial \mathbf{B}}{\partial t} = \mu_0 \left(\frac{\partial \mathbf{J}}{\partial t} + \frac{\partial^2(\epsilon_0 \epsilon(\omega) \mathbf{E} + \mathbf{P})}{\partial t^2} \right) \tag{37}$$

Finally, we replace the time derivative of $\mathbf{B}$ from Equation 32 into Equation 37 and use the fact that $\epsilon_0 \mu_0 = 1/c^2$ to get the following equation:

$$\nabla^2 \mathbf{E} - \boldsymbol{\nabla}(\boldsymbol{\nabla} \cdot \mathbf{E}) - \frac{\epsilon(\omega)}{c^2} \frac{\partial^2 \mathbf{E}}{\partial t^2} = \mu_0 \left(\frac{\partial \mathbf{J}}{\partial t} + \frac{\partial^2 \mathbf{P}}{\partial t^2} \right) \tag{38}$$

Now we can insert the relative equations for the variables $\mathbf{E} = \hat{\mathbf{E}}(\mathbf{r}, \omega, z) e^{-i\omega t}$, $\mathbf{J} = \hat{\mathbf{J}}(\mathbf{r}, \omega, z) e^{-i\omega t}$, $\mathbf{P} = \hat{\mathbf{P}}(\mathbf{r}, \omega, z) e^{-i\omega t}$. Here, we can make this approximation since laser light is monochromatic, and therefore only has these dependence on time. Moreover we emphasize that $\hat{E}(r, w, z), \hat{P}(r, w, z), \hat{J}(r, w, z)$ represent the envelope of the respective field solutions. Implementing this in the previous equation and using the fact that $\epsilon(\omega) = n^2(\omega)$, we get,

$$\nabla^2 \hat{\mathbf{E}} - \boldsymbol{\nabla}\left(\boldsymbol{\nabla} \cdot \hat{\mathbf{E}}\right) + \frac{n^2(\omega)\omega^2}{c^2} \hat{\mathbf{E}} = \mu_0 \left(-i\omega \hat{\mathbf{J}} - \omega^2 \hat{\mathbf{P}} \right) \tag{39}$$

This is the general vectorial equation of the propagation of the envelope through the medium. We can however, under approximations, turn the previous vectorial equation into a scalar one.

Firstly, we consider the electric field to be linearly polarised in a transverse direction with respect to the propagation direction. Our assumption implies that the electric field and the electric responses ($\mathbf{J}$ and $\mathbf{P}$) are transverse as well. By this assumption we can neglect the term $\boldsymbol{\nabla}(\boldsymbol{\nabla} \cdot \mathbf{E})$ in our equation. It is important to note that the validity of this assumption only remains until the beam is not very strongly focused, as if the beam aperture (the ratio between the beam diameter and the focal distance) is greater than a certain threshold, there exists a contribution of a longitudinal component of electric field E_z which would make our polarisation assumption invalid. Taking this assumption we can write our Equation 39 with respect to the projection in the transverse direction thus making the equation a scalar one.

$$\left(\frac{\partial^2}{\partial z^2} + \nabla_\perp^2 \right) \hat{\mathrm{E}} + \frac{n^2(\omega)\omega^2}{c^2} \hat{\mathrm{E}} = \mu_0 (-i\omega \hat{\mathrm{J}} - \omega^2 \hat{\mathrm{P}}) \tag{40}$$

Here we note the fact that the free charge current is equivalent to a time derivative of the non-linear polarization i.e. $\mathbf{J} \leftrightarrow \frac{\partial \mathbf{P'}}{\partial t}$ or $\hat{\mathbf{J}} \leftrightarrow -i\omega \frac{\partial \hat{\mathbf{P}}'}{\partial t}$. In this context, $\hat{\mathrm{P}}'$ and $\hat{\mathrm{J}}$ represent the Fourier transforms of

the non-linear polarization and current, respectively from the temporal space to the frequency space. As mentioned previously, since we only deal with lasers of intensities $\sim 10^{15}$ Wcm^{-2}, we do not deal with this non-linear component

Our equation then becomes:

$$\left(\frac{\partial^2}{\partial z^2} + \nabla_\perp^2\right)\hat{\mathrm{E}} + \frac{n^2(\omega)\omega^2}{c^2}\hat{\mathrm{E}} = -\mu_0\omega^2\hat{\mathrm{P}} \tag{41}$$

We note the dispersion relation $k(\omega) = n(\omega)\omega/c$ and derive the propagation equation by separating the forward and backward propagating waves:

$$(\frac{\partial}{\partial z} + ik(\omega))(\frac{\partial}{\partial z} - ik(\omega))\hat{E} = -\mu_0\omega^2\hat{P} - \nabla_\perp^2\hat{E} \tag{42}$$

using the linearity of $\hat{P}$, we get:

$$(\frac{\partial}{\partial z} + ik(\omega))(\frac{\partial}{\partial z} - ik(\omega))\hat{E} = -\epsilon_0\chi(\omega)\omega^2\hat{E} - \nabla_\perp^2\hat{E} \tag{43}$$

For the homogeneous solution we get that the solution would be a superposition of forward and backward propagating waves. It is important to note here that this solution is for the case when the right hand side of the Equation 39 is zero:

$$\hat{E} = \hat{A}_+ exp(ik(\omega)z) + \hat{A}_- exp(-ik(\omega)z) \tag{44}$$

Here we can transform the equation into a forward propagating equation by making the assumption that $|\hat{A_-}| << |\hat{A_+}|$. This assumption allows us to say that $\partial z + ik(w) \approx 2ik(w)$. By the approximation, we extend our equation with respect to the original equation 42 as:

$$2ik\frac{\partial}{\partial z}\hat{E} + 2k^2(\omega)\hat{E} = -\mu_0\epsilon_0\chi(\omega)\omega^2\hat{E} - \nabla_\perp^2\hat{E} \tag{45}$$

$$2ik\frac{\partial}{\partial z}\hat{E} + 2n(\omega)^2\omega^2\hat{E}/c^2 = -\mu_0\epsilon_0(n(\omega)^2 - 1)\omega^2\hat{E} - \nabla_\perp^2\hat{E} \tag{46}$$

$$2ik\frac{\partial}{\partial z}\hat{E} + 2n(\omega)^2\omega^2\hat{E}/c^2 = -\nabla_\perp^2\hat{E} - \mu_0\epsilon_0(n(\omega)^2 - 1)\omega^2\hat{E} \tag{47}$$

Thus we get the equation:

$$2ik\frac{\partial}{\partial z}\hat{E} + 2n(\omega)^2\omega^2\hat{E}/c^2 = -\nabla_\perp^2\hat{E} - k^2(n(\omega)^2 - 1)\hat{E} \tag{48}$$

We can also write our previous equation as follows:

$$2ik(\frac{\partial}{\partial z}\hat{E} + n\frac{\partial}{\partial t}\hat{E}/c) = -\nabla_\perp^2\hat{E} - k^2(n(\omega)^2 - 1)\hat{E} \tag{49}$$

We now change our frame from a laboratory frame to that of the frame attached to the beam i.e. from $(z,t) \to (\zeta,\tau)$ where τ is the retarded time with respect to the frame of the pulse:

$$z' = z, t' = t - z/c \tag{50}$$

Here we can now write our equation 11:

$$(\frac{\partial^2}{\partial(z')^2} + \nabla_\perp^2)\hat{E} + 2ik\frac{\partial\hat{E}}{\partial z'} - \frac{2}{c}\frac{\partial}{\partial z'}\frac{\partial}{\partial t'}\hat{E} = -k^2(n(\omega)^2 - 1)\hat{E} \tag{51}$$

We can simply the equation to the following:

$$\nabla_\perp^2\hat{E} + 2ik\frac{\partial}{\partial z'}(1 - \Phi)\hat{E} = -k^2(n(\omega)^2 - 1)\hat{E} \tag{52}$$

where $\Phi = i(\omega^{-1}\frac{\partial}{\partial t'} - (2k)^{-1}\frac{\partial}{\partial z'})$. Now, for the paraxial approximation the term $\Phi\hat{E}$ is very small thus, $\hat{E} - \Phi\hat{E} \approx \hat{E}$. Thus we have the desired relation:

$$\nabla_\perp^2\hat{E} + 2ik\frac{\partial}{\partial z'}\hat{E} = -k^2(n(\omega)^2 - 1)\hat{E} \tag{53}$$

B.1 Numerical implementation of spectral method

The following discretization method is reproduced from [3], with u being changed to E and $\hat{U}$ being changed to $\mathcal{E}$.

Thanks to the availability of generic fast Fourier transforms (FFT, FFT^{-1}) algorithms, allowing us to calculate the discretized versions of $(Eq.FT)$ and $(Eq.FT^{-1})$, the above development suggests how to compute the solution $E(z,t)$.

Let us first discretize both time and space as follows:

$$t_n = n\Delta t, \quad n = 0, \ldots, N_t - 1,$$
$$z_j = j\Delta z, \quad j = 0, \ldots, N_z - 1,$$

Our ultimate goal is to construct a numerical method that allows us to approximate the unknown analytic solution $E(z,t)$ reasonably well in these discrete grid points. That is, we want to construct a method that computes values $\mathcal{E}(j\Delta z, n\Delta t)$ (note: cursive $\mathcal{E}$) so that

$$\mathcal{E}(j\Delta z, n\Delta t) \approx E(j\Delta z, n\Delta t)$$

As a shorthand we will write $\mathcal{E}_j^n = \mathcal{E}(j\Delta z, n\Delta t)$ and (j,n) to refer to grid point $(j\Delta z, n\Delta t)$.

The variable $\hat{\mathcal{E}}(j\Delta k, n\Delta t)$ denotes the discretized version for the Fourier transformed function $\hat{E}(k,t)$. A suitable discretization of the spectral space for wavenumbers k reads:

$$k_j = j\Delta k, \quad j = -N_z/2, \ldots, N_z/2 - 1, \qquad \Delta k = \frac{2\pi}{N_x \Delta z}$$

The critical Nyquist (wavenumber) frequency ($k_c = 2\pi f_c$) $f_c = \frac{1}{2\Delta z}$

C Acknowledgement:

We thank Prof. Arnaud Couairon for his support throughout the entirety of the project. His expertise and guidance has been invaluable in shaping our work. We are highly honored to have had the opportunity to learn under their mentorship.

D Contributions

Manon Pawlowski communicated with the reviewer and the reviewee groups. She worked on the application of LLR, and contributed to proof-read the report.

Tamar Tsikarishvili made additional contributions to the report.

Aayam Basnet wrote the algorithms for the simulations and portion of the report.

Shreeya Upadhyay wrote portion of the algorithms for the simulation and the majority of the report.

References

1. Basu, Sukanta. "A simple approach for estimating the refractive index structure parameter (Cn2) profile in the atmosphere." Optics letters 40.17 (2015): 4130-4133.
2. Couairon, Arnaud, et al. "Practitioner's guide to laser pulse propagation models and simulation: Numerical implementation and practical usage of modern pulse propagation models." The European Physical Journal Special Topics 199.1 (2011): 5-76.
3. Couairon, Arnaud. "Numerical Integration of Advection-diffusion Equations." Course Jupyter Notebook file.
4. Craster, Richard V., and Roberto Sassi. "Spectral algorithms for reaction-diffusion equations." arXiv preprint arXiv:1810.07431 (2018).
5. Fleck, Jr A., J. R. Morris, and M. D. Feit. "Time-dependent propagation of high energy laser beams through the atmosphere." Applied physics 10 (1976): 129-160.
6. Frehlich, Rod, et al. "Estimates of Cn2 from numerical weather prediction model output and comparison with thermosonde data." Journal of Applied Meteorology and Climatology 49.8 (2010): 1742-1755.

7. Kulikov, Victor Alexeevich, et al. "Method of estimation of turbulence characteristic scales." Applied optics 51.36 (2012): 8505-8515.
8. Laurila, S. H. "Statistical analysis of refractive index through the troposphere and the stratosphere." Bulletin Géodésique (1946-1975) 92 (1969): 139-153.
9. Lawrence Livermore National Laboratory. "Building the World's Largest Laser." `https://lasers.llnl.gov/10-years-of-dedication/building-nif`
10. Martin, J. M., and Stanley M. Flatté. "Intensity images and statistics from numerical simulation of wave propagation in 3-D random media." Applied Optics 27.11 (1988): 2111-2126.
11. Merkowitz, Stephen M. "Tests of Gravity Using Lunar Laser Ranging". **Living Reviews in Relativity**, (2010) 13 (1): 7
12. Paschotta, Rüdiger. "Gaussian Beams." `https://www.rp-photonics.com/gaussian_beams.html`
13. Raj, A. Arockia Bazil, J. Arputha Vijaya Selvi, and S. Durairaj. "Comparison of different models for ground-level atmospheric turbulence strength (Cn 2) prediction with a new model according to local weather data for FSO applications." Applied optics 54.4 (2015): 802-815.
14. Sherratt, Jonathan A. "A comparison of two numerical methods for oscillatory reaction-diffusion systems." Applied Mathematics Letters 10.2 (1997): 1-5.
15. Steigerwald, William. NASA: laser beams between earth and moon boost science, August 2020
16. Tatarskii, Valerian Ilitch. "The effects of the turbulent atmosphere on wave propagation." Jerusalem: Israel Program for Scientific Translations, 1971 (1971).
17. Twomey, Sean, Herbert Jacobowitz, and Hugh B. Howell. "Light scattering by cloud layers." Journal of Atmospheric Sciences 24.1 (1967): 70-79.
18. Zhang, Dai, et al. "Atmospheric turbulence phase screen modeling method based on sub-bands division and multirate sampling." Optik 163 (2018): 72-80.